

"MARS-3": INFRARED TEMPERATURES AND THERMAL  
PROPERTIES OF THE PLANET'S SURFACE

V. I. Moroz, L. V. Ksanfomaliti, G. N. Krasovskiy,  
V. D. Davydov, N. A. Parfent'yev, V. S. Zhegulev  
and G. F. Filippov

(NASA-TT-F-15914) MARS-3: INFRARED  
TEMPERATURES AND THERMAL (Techtran Corp.)  
41 p HC \$3.75 CSCI 03A

N75-15573

Unclass

G3/91 07402

Translation of: "Mars-3": Infrakrasnyye Temperatury  
i Teplovyye Svoystva Poverkhnosti Planety, Pr-172,  
Institute of Space Research, Academy of  
Sciences USSR, Moscow, 1974, 51 pages



1. Report No. NASA TT F-15,914	2. Government Accession No.	3. Recipient's Catalog No.	
4. Title and Subtitle "MARS-3": INFRARED TEMPERATURES AND THERMAL PROPERTIES OF THE PLANET'S SURFACE		5. Report Date DECEMBER 1974	
		6. Performing Organization Code	
7. Author(s) V. I. Moroz, L. V. Ksanfomaliti, G. N. Krasovskiy, V. D. Davydov, N. A. Parfent'ev, V. S. Zhegulev and G. F. Filippov		8. Performing Organization Report No.	
		10. Work Unit No.	
9. Performing Organization Name and Address Techtran Corporation P.O. Box 729 Glen Burnie, Maryland 21061		11. Contract or Grant No. NASW-2485	
		13. Type of Report and Period Covered Translation	
12. Sponsoring Agency Name and Address NATIONAL AERONAUTICS AND SPACE ADMINISTRATION WASHINGTON, D.C. 20546		14. Sponsoring Agency Code	
15. Supplementary Notes  Translation of: "Mars-3": Infrakrasnyye Temperatury i Teplovyye Svoystva Poverkhnosti Planety, Pr-172, Institute of Space Research, Academy of Sciences USSR, Moscow, 1974, 51 pages			
16. Abstract  The pamphlet describes the infrared radiometer installed on Mars-3 and outlines the results of six series of observations from 15 December 1971 to 28 February 1972. Conclusions on the thermal properties and physical structure of the Martian terrain are outlined; these are, the authors note, in substantial agreement with the results of similar observations made by Mariner-9.			
17. Key Words (Selected by Author(s))		18. Distribution Statement  Unclassified-Unlimited	
19. Security Classif. (of this report) Unclassified	20. Security Classif. (of this page) Unclassified	21. No. of Pages 40	22. Price

# "MARS 3": INFRARED TEMPERATURES AND THERMAL PROPERTIES OF THE PLANET'S SURFACE

V. I. Moroz, L. V. Ksanfomaliti, G. N. Krasovskiy,  
V. D. Davydov, N. A. Parfent'yev, V. S. Zhegulev,  
and G. F. Filippov

## 1. Introduction

The brightness of Mars in the wavelength region  $\lambda > 5$  is determined by the thermal radiation of the surface. Using the brightness of Mars in the infrared region of the spectrum, it is possible to estimate the temperature of the uppermost ground layer and to obtain data on its thermal properties and, indirectly on its structure. /4\*

By telescopes on Earth, Mars was observed with this purpose in mind in the 8-14  $\mu$  range, in which the Earth's atmosphere is ~~relatively~~<sup>sufficiently</sup> transparent [1-5]. Sinton, as a result of analysis of measurements carried out with the 5-meter reflector of the Mount Palomar Observatory during the opposition of 1954, obtained the first estimates of the thermal inertia of Martian soil as a whole [4]. In a number of works attempts have been made to refine these estimates by performing detailed calculations on thermal models. However, to achieve further significant progress it was necessary to improve the quality of the initial observation material considerably.

It is the ~~most~~<sup>very</sup> difficult to overcome the limitations of spatial resolution. The observations of Sinton and Strong were carried out with a 1.5" diaphragm at an angular diameter of Mars of around 25"; this corresponds to 400 kilometers on the planet's surface (in the center of the disc). Atmospheric vibration can double this value and so it is impossible to improve spatial resolution noticeably when making observations from Earth. It should be noted that making these observations from balloon-mounted telescopes or from orbit around Earth would be of no help in this respect because the diffraction limit of a metric telescope at 10  $\mu$  is around 2". At the moment there are no telescopes with larger

---

\*Numbers in the margin indicate pagination in the foreign text.

diameters on stratospheric or space platforms. A radical solution to the problem is obtained by placing an infrared radiometer on board an unmanned space station which operates in the immediate vicinity of the planet. The first attempt of this type, which was undertaken by the fly-by space stations Mariner 6 and 7 in 1969, made it possible to obtain basically new results [9]. Artificial satellites of Mars considerably broaden the possibility of experimentation, and all three of the first orbital stations near Mars, the Soviet Mars-2 and Mars-3, and the American Mariner-9 had among their scientific equipment infrared radiometers with which to measure the intensity of the planet's thermal radiation [10,11]. In the following we will give a brief description of the instrument mounted aboard the Soviet artificial satellites of Mars, the measurement method used, and the results obtained by Mars-3. /5

## 2. Infrared Radiometer

An optical diagram of the radiometer is presented in Figure 1. The flux of infrared radiation from the planet passes through diaphragm D (with an aperture of  $13 \text{ cm}^2$ ), is reflected by diagonal mirror R, and is focused by a segment of the off-axis parabolic mirror  $R_2$  in the plane of diaphragm  $D_3$ . The diameter of the diaphragm aperture is 1.2 mm; this corresponds to an angular field of vision of around 0.025 rad. A symmetrically arranged second channel (mirror  $R_3$  - diaphragm  $D_2$ ) isolates the same field, which is turned toward outerspace. The foci of both parabolas coincide. Modulator M is an opaque disc which vibrates at a frequency of 16 Hz and covers each of the channels in turn; this leads to the appearance of a variable component in the current which reaches the receiver. The indium antimonide filter mounted behind diaphragm  $D_3$  cuts off the shortwave portion of the radiation with a wavelength of less than  $8 \mu$ . The receiver R is a low-resistance nickel bolometer with a threshold sensitivity of around  $10^{-9} \text{ watt} \cdot \text{Hz}^{-1/2}$ .

Calibration disc K is periodically (at intervals of 36 seconds and 4 seconds) introduced into the channel and is directed at the planet to check the stability of the instrument's sensitivity while it is making measurements. The thermal conditions of the radiometer are monitored by 2 thermistors, one of which is fastened to disc K, and the second to the bolometer mount. An optical diagram with two off-axis parabolas and an opaque modulator was used earlier in /6

measurement of the infrared temperature of the Earth's surface from the "Kosmos-149" satellite [12] and was suggested for use as the Martian radiometer by A. M. Kasatkin.

A functional diagram of the instrument's electronic component is shown in Figure 2. The low output resistance of the bolometer is matched to the circuit by using a low-noise transformerless preamplifier PU. From narrow-band filter — UPF the signal moves to terminal amplifier OU, and from the latter to synchronous doubler SU. The signal, which is proportional to the input current, then moves to the telemetry.

Control generator ZG generates a pulsed voltage with a frequency of 32 Hz. Beyond frequency divider DC, the signal moves to modulator unit UM and reference voltage generator GON which feeds the synchronous doubler SU.

The total amplification of the channel is around  $10^7$ . The noise brought to the 30 Ohm input is  $10^{-9}$  volts at an output circuit time constant of around 0.5 sec. A more detailed electrical diagram of the instruments is given in [13].

The infrared radiometer is a small, economical instrument. Its full weight is 1.20 kg, and its feeder circuit consumption does not exceed 290 ~~mvt.~~ <sup>milliwatt</sup>.

A diagram of the radiometer's directivity was investigated by using a radiation source set up at a distance of 25 meters from the instrument and shifted in two mutually perpendicular directions. The diameter of the radiation source was 80 mm. The results of the measurements are presented in Figure 3. The width of the diagram at a level of 0.5 from the maximum is 0.025 to 0.030 rad (the diagram exhibits deviations from the central symmetry of the order of 20%). At a distance of 1500 km from the surface of the planet, this corresponds to linear dimensions of 40 to 45 kilometers. The "wings" of the diagram were measured to a level of 2% of the maximum. The directivity diagram was investigated by using a laboratory model of a radiometer completely identical to the instruments set up on board the spacecraft. The time constant of the instrument was approximately 1 second. /7

In Figure 4 we have presented the spectral characteristics of a typical model of an indium antimonide filter which was used in the radiometers. Unfortunately, it was not possible to investigate the spectral characteristics

of the instrument as a whole. It may differ from the spectral characteristics of the filter owing mainly to the selectivity of the absorption coefficient of the black covering the bolometric disc. A considerable drop in the absorption coefficient is to be expected in the wavelength range exceeding  $40 \mu$ , although it can take place on shorter waves as well. The mirror optics of the radiometer has an aluminum coating, the reflection coefficient of which is practically independent of the wavelength over the entire infrared region of the spectrum.

Laboratory calibration on the brightness temperature was carried out using two identical conic models of an absolutely black body (abb) set up in front of each channel. The abb in front of the "Kosmos" channel was cooled by liquid nitrogen to a temperature of around  $100^\circ \text{K}$ , and the temperature of the second abb varied between  $120$  and  $300^\circ \text{K}$ . In Figure 5 curve a is the laboratory calibration curve for the radiometer mounted on "Mars-3". The temperatures of the abb for the "planet" channel are plotted on the X-axis. Curve b is the theoretical calibration curve calculated on the assumption that the spectral characteristics of the radiometer are determined mainly by the filter (Figure 4, broken line). Curves a and b agree sufficiently well in the area of relatively high temperatures ( $250$  to  $300^\circ \text{K}$ ) but diverge noticeably in the range of the lower temperatures (the calculated curve is higher than the measured one). This is explained most easily by lowering of the black absorption coefficient as wavelength increases.

/8

The relative error in measuring the current for the "Mars-3" radiometer together with the telemetry system ranges from  $\pm 2-3\%$  for intensity temperatures of  $250$  to  $270^\circ \text{K}$ . This value was estimated directly from the results of the measurements. The error of  $\pm 2\%$  in the flow corresponds to an error of  $\pm 1.5^\circ$  in the brightness temperature at  $T = 250^\circ \text{K}$ . The lower limit of the brightness temperatures recorded by the "Mars-3" radiometer was around  $160^\circ \text{K}$ . Under laboratory conditions the sensitivity threshold was approximately  $145^\circ \text{K}$ , but on board it was not reached because of the fact that the instruments' temperature was too low, and this caused a twofold lowering of sensitivity in comparison to the sensitivity measured in the laboratory. The electrical noise at the instrument output was so small that it was not recorded by the telemetry system.

The infrared radiometer, like the other instruments in the astrophysical complex [14, 15], was firmly attached to the body of the unmanned space station, and its orientation in a constant direction was ensured by the general system of solar-stellar orientation. When the spacecraft approached the pericenter of its orbit, the instruments were switched on by a special optical sensor several minutes before crossing the limb. The optic axes usually intersected the planet along a line which was close to a great circle, and the transition from limb to limb took about 30 minutes. We will henceforth call the path of the optical axis on the surface of the planet the measurement path according to a preliminary estimate; the precision with which the measurement path was determined was 1 to 2 degrees in the aerographic coordinates. The position of the "Mars-3" measurement paths on the planet's surface is shown in Figure 6.

The distance at the pericenter on the surface of Mars varied somewhat with the evolution of the orbit, ranging over the period in question from approximately 1500 to 1000 kilometers. The first two passes, on 15 and 17 December 1971, took place during a dust storm, the third (9 January) was evidently not yet free from the effect of the storm, and the others (3, 16, and 28 February, 12 March) took place after the dust storm was over. In December, January, and February, the measurement path which corresponded to the successive data of the pass around Mars, varied relative to one another by approximately  $90^\circ$  in longitude. As a result, considerable portions of the February paths ran near the measurement paths of December and 9 January, and we have measurements for the same areas of Mars which were obtained during the storm (or, more precisely, during its last stages) and after the storm. For a variety of reasons, we have not yet succeeded in reliably relating the 12 March path to the surface to a sufficient extent, and its position as indicated in Figure 6 should be regarded as a tentative one.

### 3. Determining the Brightness Temperature of the Planet $T_b$

The laboratory calibration curve can be used to calculate the brightness temperatures of Mars if it is assumed that a given output signal value corresponds to a known brightness temperature. For the purposes of the experiment, it was proposed to use the calibration disc as an intermediate standard. However,

analysis of the results showed that the brightness temperatures of the planet obtained by this method are consistently lower than that obtained by observation from Earth and by "Mariner" in 1969.

At first it was difficult to calculate the magnitude of the error since, during the first passes of "Mars-3", there was on the planet a dust storm which lowered the temperature of the surface somewhat in comparison to the normal conditions on the planet. After the dust storm was over, it became clear that there remained a consistent difference (12 to 15°) between the brightness temperatures of "Mars-3" and previous observations. The probable cause is that solid angle  $\omega$  within which radiation from the calibration disc is received is greater than the angle for planetary radiation  $\Omega$ . If there occurs a difference in temperature between the disc and the planetary channel tube, then a consistent error in the brightness temperature of the planet occurs which is opposite in sign and equals

/10

$$\Delta T \approx \Delta T_0 \left( \frac{\Omega}{\omega} - 1 \right), \quad (1)$$

where  $\Delta T_0$  is the difference in the brightness temperature of the calibration disc in the part of the tube covered when the disc is introduced into the optical path. The temperature of the calibration disc was consistently 4 to 6° higher than the temperature of the bolometer mounting. If the latter is equal to the temperature of the tube, then there should be a consistent error near the value indicated above.

A constant correction of  $\pm 12^\circ$  was adopted for the brightness temperature of the calibration disc. The value of this correction provides the best agreement with the terrestrial [3, 4] and Mariner (II) results for the equatorial regions at noon after a correction is made for atmospheric absorption (see below).

During the observation period the measured temperature of the calibration disc ranged from 253 to 260° K. During each half-hour observation session, it remained constant within the measurement error limits ( $\pm 2^\circ$ ). The sensitivity of the radiometer remained constant within the limits of 30% from session to session and 10% during each session (a 10% increase in the calibration disc reading usually took place within the first 10 to 15 minutes). These values

are correct if the radiometer sensitivity is proportional to the calibration disc readings. A necessary condition is consistency of difference  $\Delta T_0$ . Otherwise systematic or continuously variable errors may occur. It is impossible to evaluate their magnitude reliably. We believe that they are within the limits of  $\pm 7\%$  relative to the flux ( $\pm 5^\circ$  at a brightness temperature of  $250^\circ$  K). /11

#### 4. Correction for Atmospheric Absorption and Radiation

The basic component of the Martian atmosphere is carbon dioxide. In the range of the basic  $\text{CO}_2$  band of  $15 \mu$ , the gas absorbs the radiation of the surface, and here in an area of a width of  $\Delta\lambda \approx 2 \mu$ , we adopt the radiation from the atmosphere determined by its temperature at the level  $\varphi = 1$ . This temperature may be either below or above the surface temperature, and accordingly the spectrum of the planet will have an absorption or an emission band. Both types of spectra were recorded by the infrared spectrometer on Mariner-9 [16].

Among the other components in the Martian atmosphere, CO and  $\text{H}_2\text{O}$  have infrared bands, but their content is very small and their role in planetary radiation negligible.

Rigorous allowance for the atmospheric contribution to the outgoing flux requires knowledge of the vertical temperature distribution at every point at which measurements were made. However, the estimates made on the basis of the Martian spectra, both measured [16] and calculated [17], have shown that the contribution of the atmosphere to the outgoing flux is within the limits of approximately 10% of its total value. Therefore, a correction for the atmosphere has been introduced as an approximation. The correction was calculated according to the formula

$$K = \frac{F_0 - F}{F_0} = W_0 \frac{1}{\sqrt{\mu}} \frac{B(T_1) - B(T_2)}{6 T_1^4 [\bar{\epsilon}_{28} - \bar{\epsilon}_0 + 0.2(\bar{\epsilon}_{45} - \bar{\epsilon}_{28})]}, \quad (2)$$

where  $F$  is the flux which the radiometer receives from the planet and  $F_0$  is the flux emitted by the surface within the range of the radiometer sensitivity;

$W_0$  is a constant, which equals the width of a  $15 \mu$  band under certain average conditions; we have taken  $W_0 = 2.25 \mu$ ; /12

$\mu$  is the cosine of the zenith distance of Mars-3 at the point observed;

$T_1$  is the brightness temperature of the surface;

$T_2$  is the brightness temperature of the atmosphere (see below);

$B(T)$  is the monochromatic brightness of an absolutely black body at a wavelength  $\lambda$  of 15 microns;

$Z_x$  is the relative portion of the total radiation flux of an absolutely black body in the wavelength range  $\lambda < x$ ;

$a$  is the relationship of the sensitivity in the spectral range of 28-45  $\mu$  to the sensitivity in the 8-28  $\mu$  range;  $a$  was taken as equal to 0.6 in accordance with the ideal spectral transmission curve of the filter (Figure 4).

The least-known quantity is  $T_2$ , i.e., the brightness temperature of the atmosphere in the 15  $\mu$  band. In reality it changes sharply within the limits of the band. We set

$$T_2 = \frac{\bar{T}_1}{\sqrt{2}}, \quad (3)$$

where  $\bar{T}_1$  is the average daily temperature of the surface at a given latitude. Formula (3) presupposes that the temperature at the base of the atmosphere is equal to  $\bar{T}_1$ , and that  $T_2$  is equal to the effective temperature of a gray, optically thin atmosphere in thermal equilibrium with the surface and outerspace. Both propositions are extremely conditional, especially the latter. Quantity  $\bar{T}_1$  is calculated from

$$\sigma \bar{T}_1^4 = \frac{E_0}{r^2} (1-A) \bar{\mu}_0, \quad (4)$$

where  $E_0$  is the solar constant,  $r$  is the radius vector of Mars,  $A$  is the albedo,  $\bar{\mu}_0$  is the average daily value of the cosine of the sun's zenith distance at the assigned value of latitude  $\varphi$  and areocentric solar declination  $\delta$ . Value  $A = 0.25$  was adopted. The stratospheric temperatures  $T_2$  calculated by this method were around 200° K for the low latitudes, and this corresponds closely to the experimental results for the 0.3 mb level obtained by Mariner-9 [16].

/13

In Section 7 the brightness temperature curves and curves in which allowance has been made for the atmosphere by using the correction calculated according to formula (2) are given for one of the measurement sessions (15 December; see Figure 9). It is evident from the agreement of these curves that the correction is in fact within the limits of 10%. The correction is positive during the daytime and negative at night. In the zone  $\pm 1^h$  from the terminator, the correction was negligibly small.

We have taken into account the contribution only of the gaseous component of the atmosphere. The aerosol components can make a noticeable contribution during a dust storm. The optical thickness of the dust during the December measurements in the region  $\lambda > 8$  micron was certainly small, but a value for it of the order of 0.1 is certainly possible.

## 5. Determination of the Kinetic Temperature of the Martian Soil

The kinetic and brightness temperatures are associated by the relation

$$\int_0^\infty \bar{B}_\lambda(T_k) S_\lambda d\lambda = \int_0^\infty \bar{B}_\lambda(T_s) S_\lambda \epsilon_\lambda d\lambda, \quad (5)$$

where  $B_\lambda$  is Planck's function,

$S_\lambda$  is the spectral characteristic of the instrument, and

$\epsilon_\lambda$  is the emissivity.

Usually one makes use of the concept of average emissivity

$$\bar{\epsilon} = \frac{\int_0^\infty \bar{B}_\lambda(T_k) S_\lambda d\lambda}{\int_0^\infty \bar{B}_\lambda(T_s) S_\lambda d\lambda} \quad (6)$$

When  $S_\lambda = \text{const}$ , a simple relationship is valid

$$\begin{aligned} \bar{\epsilon} &= \left( \frac{T_k}{T_s} \right)^4, \\ T &= \frac{T_k}{\sqrt[4]{\bar{\epsilon}}} \end{aligned} \quad (7)$$

from which we derive

In the case of such a wide spectral characteristic, such as that of our radiometer, this relationship should be in effect satisfied. In this process an error in  $\epsilon$  of even 10% gives a total error in temperature of 2.5%. Evaluation of the average emissivity of natural silicate materials can be made on the basis of data of measurement of their reflectivity in the infrared range [18,19]. The measurement results available to us refer only to the  $\lambda < 25 \mu$  range, but this should not cause great indefiniteness, since in this range more than 65% of all energy is emitted at  $T \geq 200^\circ \text{K}$ . Since, as the results of radiometric observations (both these and others published earlier) have shown, the structure of the soil is mainly fine-grained, one can hardly expect considerable increase in the reflection coefficient in the individual spectral ranges due to the effects of residual rays. Using the results of the laboratory measurements indicated above as a basis, we have adopted

$$\epsilon = 0.9. \quad (8)$$

In [9] it was found that the best internal agreement of the Mariner measurements in the 10 and 20  $\mu$  ranges occurred at

$$\epsilon = 0.88 \pm 0.03 \quad (9)$$

for 20  $\mu$  if we take the estimate of (8) for 10  $\mu$ . This indicates that the dependence of the radiation coefficient on the wavelength in the spectral range with which we are concerned is relatively small.

The radiation coefficient of real bodies depends on the direction. Pettit and Nichol森 have investigated this relationship for the Moon (see Figure 7, [20]). This relationship can be presented in the form

$$\epsilon = \epsilon_0 \mu^q$$

where  $q = 0.25$ . According to [9],  $q = 0.1$  for Mars, and this has been adopted in this work. In the majority of the points observed, this correction is negligibly small (of the order of 1%), but near the limb and the terminator, it may be considerable (up to 10% relative to the flux).

/15

## 6. Thermal Models

Surface temperature  $T_s$  is determined by a balance of four processes:

1. absorption of solar radiation,
2. surface emission,
3. heating and cooling of the soil due to thermal conductivity,
4. heat exchange with the atmosphere.

If one disregards process (4), the equation of thermal balance may be written in the form

$$\epsilon \sigma T_s^4 = E(1-A) + F_0 \quad (10)$$

where  $E$  is illumination; by day  $E = \frac{E_0}{2} \cos \theta$ , by night  $E = 0$ ; the flux in the soil

$$F = -K \frac{\partial T}{\partial z} \quad (11)$$

$K$  is the thermal conductivity coefficient;  $z$  is a coordinate read vertically down from the surface.

Flux  $F$  is determined by thermal conductivity

$$\frac{\partial F}{\partial z} = K \frac{\partial^2 T}{\partial z^2} = \rho c \frac{\partial T}{\partial t} \quad (12)$$

where  $c$  is the specific heat per unit mass, and  $p$  is the density. Equation (10) serves as the boundary condition for equation (12). Wesselink [21] and Jaeger [22, 23] examined the solution of the latter as it applied to the surface of the Moon and the planets. Wesselink [21] has shown that the time dependence is determined unambiguously by three parameters:  $\epsilon, A, I = (kpc)^{1/2}$

The latter quantity may be termed thermal inertia. The greater is  $I$ , the higher are the nighttime temperatures and the greater is the lag of the daytime temperature maximum of the surface behind noon maximum  $E$ . In this process the penetration depth of the first harmonic of the thermal wave is

$$\ell = \sqrt{\frac{k}{\rho c} \frac{P}{\pi}}, \quad (13)$$

where  $P$  is the rotation period; at depth  $\ell$  the amplitude of the first harmonic of the temperature fluctuations damps  $e$  times. For terrestrial eruptive rocks  $I = 0.05$ , and for fine dust in a vacuum around  $0.001 \text{ cal} \cdot \text{cm}^{-2} \cdot \text{sec}^{-1/2} \cdot \text{deg}^{-1}$ .

For each measurement path of Mars-3, theoretical temperatures were calculated at the following albedo and thermal inertia:

$$A = 0.15; 0.25$$

$$I = (kpc)^{1/2} = 0.004; 0.006; 0.008 \text{ cal} \cdot \text{cm}^{-2} \cdot \text{sec}^{-1/2} \cdot \text{deg}^{-1}.$$

The calculation was made by the Laplace transform method with the day divided into 20 intervals and by use of the coefficient given in the paper by Jaeger [23]. The emissivity chosen was  $\epsilon = 0.9$ . The results of calculation for 9 January 1972 are given as an example in Figure 7. A thermal chart of the planet within the latitude limits of  $\pm 60^\circ$  was calculated for each date, and the data for the path were taken from the chart. In a number of cases further processing required extrapolation and greater albedo values. This extrapolation for daytime was performed by multiplying the flows obtained at  $A = 0.25$  by the coefficient  $(I-A)/0.75$ , where  $A$  is the new albedo value. For several dates thermal charts were calculated by use of the Wesselink method: the initial distribution of  $T(z,0) = \text{const.}$  was assigned, and the value  $T(z,t)$  was calculated for the constantly increasing values of  $t$  until the latter became a periodic function with a precision of  $1^\circ$ . The agreement between the two methods is satisfactory.

/16

Figure 7 shows how the variations in thermal inertia constant affects the temperatures. Around mid-day in the former increase lowers the temperature, and increases it near the evening terminator (and at night). Increase in the albedo at constant thermal inertia leads to decrease in temperatures at any time during the rotation of the planet.

On the very same measurement paths other instruments on board Mars-3 obtained photometric profiles at several wavelengths from 0.37 to 1.4  $\mu$  [14, 15]. Contrasting these profiles with the brightness temperature makes it possible, when comparing them with the observational data, to single out the effects of the albedo and thermal inertia variations along the paths. It remains for us to consider the possible influence of variations in emissivity, which cannot be estimated on the basis of the available observational data. Figure 8 shows that the influence of  $\epsilon$  on the value of the outgoing flux and the brightness temperature is very slight. At  $F = 0$  it obviously should not take place at all. If  $F$  is taken into account, as we see, the effect is 1-2° in daytime. Thus if on the daylight part of the path the brightness temperatures in 2 adjoining areas differ by 5 to 10°, then the cause can only be a difference in albedo or thermal inertia. In addition, the kinetic temperature in these two regions may, generally speaking, prove to be the same or, on the other hand, may vary even more greatly, depending on what is their relative emissivities are.

Leovy [6], Gierash and Goody [24], and Meugebauer et al [9] have discussed the role of heat exchange with the atmosphere. In equation (10) in the last-named paper a constant term equaling 0.01 of the mid-day insolation value was added as an atmospheric correction. It is probable that in reality the correction should be larger, and this problem merits further individual examination. Here we restrict ourselves to two models which do not allow for the influence of heat exchange with the atmosphere on the surface temperature. We merely note that taking it into account would increase the value of  $I$  found by comparing the models with observations of the daytime portion of the path. The estimates of  $I$  for the nighttime regions, on the other hand, would be decreased.

A radiometric albedo of 0.25 was chosen as being near the spherical integral albedo of the planet (0.26 according to [25] and 0.25 according to [26]). It

/17

/18

is assumed that the albedo is characteristic on the average for the light regions. 0.15 is accordingly the typical value for the dark regions. It should be noted that in fact the radiometric albedo of the local regions is equal to the "plane" albedo, and not the spherical. The "plane" albedo is the relationship of the radiation flux scattered over a plane area to the flux of parallel rays which strike it. Its value depends on the angle of incidence. In a series of papers McCord et al [27-31] have presented the results of spectral electrophotometric study made on Earth of the dark and light regions on Mars. From these observations it is also impossible to obtain the necessary value of the "plane" albedo; they give only the normal albedo (the normal brightness coefficient). For a Lambert surface, however, the spherical, plane, and normal albedos are equal to each other, and, since in the region of  $\lambda > 0.8 \mu$  the photometric properties of the surface of Mars approach those required by Lambert's law, it is possible to use the values of the normal albedo instead of the "plane" one. The region of  $\lambda > 0.8 \mu$  gives a contributes approximately 60% to the integral albedo.

It must be noted that in the article by McCord et al [27-31], no clear distinction is made between the concepts of normal and geometric albedos. The  $A = 0.40$  chosen for the light regions in the work of Neugebauer et al [9] was an overestimate for this very reason. The authors [9] multiplied the supposedly "geometric" albedo of McCord by the phase integral (approximately 1.5 for the region of  $\lambda > 0.8 \mu$ ), but it is not necessary to do so because this is not a geometric albedo. When going from a normal albedo to a geometric one, it is necessary to take into account the darkening which takes place towards the edges, but this was not done (see [30]).

## 7. Measurements Results and Analysis of Results

/19

Figures 9-14 show the results of measurements for 6 Mars-3 observation sessions, from 15 December 1971 to 28 February 1972. The heavy continuous line is the initial radiometer signal as a function of Moscow time  $t_m$ . The signal was proportional to the flux of radiation to the bolometer (scale on the right) with a correction which allowed for the contribution by the Martian atmosphere (see Section 4). On the left are the scales of the brightness temperature and kinetic temperature of the surface; the procedure for obtaining these temperatures

was discussed in Sections 3 and 5. The broken line in Figure 9 (15 December 1971) gives the flux without correction for the atmosphere. The continuous sections of the fine line with the 2 numbers accompanying them are the temperatures as calculated according to the models (Section 6); the first number gives the albedo, and the second the parameter of thermal inertia  $I = (\text{kpc})^{1/2}$ . The fine continuous line is the photometric profile (brightness in relative units) along the same path, as measured by the  $\text{H}_2\text{O}$  photometer of Mars-3 in the continuous spectrum channel [32]. They refer to a wavelength of  $1.4 \mu$ . It is well known that the contrast between seas and continents reaches a maximum at around  $\lambda = 0.8 \mu$ , and as the wavelength is further increased, remains practically unchanged (see, for instance, [30]), while the heavy solid line reflects a change in the thermal radiation flux of the planet along the path, and the fine line similarly shows change in the flux of reflected solar radiation. In Figure 15 (16 February 1972) the part of the photometric profile in the near ultraviolet region of the spectrum is indicated by a broken line. This line indicates the increase in brightness caused by clouds in the high latitudes.

Two vertical hatchmarks show the width of the radiometer directivity diagram on the  $t_m$  scale for various moments in time. The directivity diagram of the  $\text{H}_2\text{O}$  photometer is approximately 4 times narrower, and this explains, at least partially, the wealth of detail on the reflected radiation curve. In principle a correction can be introduced into the observed profile for the final width of the directivity diagram, but for the moment this has not been done.

/20

It is worthwhile to begin review of the material with the last three passes, i.e., 3, 16, and 28 February, since they are apparently completely free from the effects of the dust storm. The first thing which strikes the eye is the negative correlation of the thermal and solar fluxes in the large (and sometimes even in the small) components of both curves.

3 February (Figure 12) is the shortest measurement session; for technical reasons it was ended long before the second limb of the planet was crossed. The sharp drop in the intensity of reflected radiation in the area of the Mare Cimmerium is accompanied by an increase in thermal radiation. These small minima in the lower curve (reflected radiation) close to the moments of 16, 17, and 18 minutes are accompanied by maxima in the upper curve. The temperature

of the light regions of Eridania and Chersonesus are described well by the models where  $A = 0.25$  and where  $I$  is within the limits of 0.006 to 0.008, and the temperature of the Mare Cimmerium requires an albedo of 0.15 and  $I = 0.006$ . The general range of surface temperature variations is around  $30^\circ$  for the path of 3 February: from  $225^\circ$  K at latitude  $-53^\circ$  near midday (Chersonesus) to  $285^\circ$  K at latitude  $-32^\circ$  on 14 February (Mare Cimmerium). A comparison of these paths with the photographs of Mars-9 and the Mariner chart of Mars [33] does not show any agreement between the topographical details and the special characteristics of the radiometric profile.

The session of 16 February (Figure 13) has been plotted almost completely (with the exception of the zone of entry onto the limb, where possibly 1 minute was lost because the instruments took some time to heat up). This path is located entirely within the daylight part of the planet -- the local solar time varies within the limits of 1100 to 1430 -- and crosses the planet from south to north, from latitude  $-50^\circ$  to  $+70^\circ$ . In the zone from  $-35^\circ$  to  $+25^\circ$ , the path crosses the belt of dark areas, namely Iapygia and Syrtis Major (this is probably the darkest of the Martian seas). The drop in albedo in the region of the belt of seas is accompanied by an increase in thermal flux. In Syrtis Major not only a decrease in albedo is required, but also a decrease in the thermal inertia parameter to 0.004 to provide agreement between the observational data and the calculated models, and in Iapygia and in the neighboring light area Noachis, the thermal inertia parameter is nearer 0.008. The surface temperature in Syrtis Major approaches  $290^\circ$  K (1400 local time). In the light region of Meroe an increase in kpc (or albedo) occurs with movement northward. The temperature drops to the lower limits of the radiometer's sensitivity ( $160^\circ$  K) near latitudes  $L = +55^\circ$  and remains this low up to  $+70^\circ$ , where the optical axis of the radiometer crossed the edge of the planet. /21

The negative correlation between the thermal and reflected fluxes is easily visible in Iapygia and Syrtis Major (the peaks of the lower curves and the trough of the upper curve are around 45 and 47.5 minutes). However, it is not possible to find a corresponding relationship for all the components of the thermal radiation curve in the reflected radiation curve. We mean by this troughs 1 and 2. In these areas there are on the Mariner chart embankments of

rather large craters (see Figure 3 [32]). The fact that their temperature is lower can be explained by the greater thermal conductivity and the density of the material in the surface layer of the embankments. In a number of cases, intersection with the craters is accompanied by troughs in the reflected radiation curve (components a - e) to which peaks of thermal flux correspond (for instance, b and e). Troughs of the reflected flux can be caused by changes in the albedo or by slopes. Unfortunately, the limited precision of the chart [33] and coordination of the paths make agreement between the topographic and the photometric less than fully certain [32].

/22

The curves of 16 and 28 February are generally similar. There are even fewer light regions on the 28th February path, and the temperature drops even more sharply in the northern latitudes (the  $160^\circ$  level reaches approximately  $L = +45^\circ$ ). The maximum temperatures (approximately  $285^\circ \text{ K}$ ) occur in the Mare Erythraeum (at 1300). The negative correlation of the thermal and reflected fluxes can be noted especially well in the region between 54 and 56 minutes (the northern boundary of the Mare Erythraeum). The trough in the thermal flux I is not accompanied by any peak in the reflected flux and is not clearly identified with the topographical details. It can be noted, nevertheless, that there are many craters near this region of the path (Figure 4 [32]).

The fast drop in temperature in the Mare Acidalium requires higher albedo values, values which are too large even for the light regions. The ultraviolet photometric profile on the paths of 16 and 28 February [34] shows a sharp increase in brightness in the area of the sharp temperature drop at the northern end of the path. This brightness drops off as the wavelength increases and completely disappears at  $1.4 \mu$ . It is natural to advance the hypothesis that this intensity is explained by clouds, the albedo of which drops as the wavelength increases (this is possible because of the small dimensions of the particles; see [35]). The photographs of Mariner-9, obtained on dates close to this (DAS 8407324, 17 February and DAS 9018844, 25 February) do in fact show clouds in the same regions of Mars where we observed an increase in UV intensity and a temperature drop. The reflection and absorption of solar radiation in the clouds could be the reason for the sharper drop in temperature than is yielded by any of the reasonable models which take into account only the properties of the surface.

It is natural to ask what source is of thermal radiation in the low temperature zone in the north: the surface or the clouds themselves? The brightness profile at  $1.4 \mu$  does not react at all to the appearance of clouds, and from this one can conclude with considerable confidence that they are optically thin in this region of the spectrum [35]. If this is true, then their optical density should be even lower in the range  $\lambda > 8 \mu$ , and the measured upper limits of thermal flux refers to the surface. It is not clear whether a condensation of  $\text{CO}_2$  takes place on the surface itself (this occurs at  $T \approx 150^\circ \text{K}$ ), especially if one judges by the  $1.4 \mu$  profile, which does not show any increase in intensity here. One can state with considerable confidence that the clouds which were spoken of earlier are condensation clouds, although the nature of the condensed material is not fully clear; it could be either  $\text{CO}_2$  or  $\text{H}_2\text{O}$ ; the latter variant seems to us to be the more likely one [35].

/23

Let us now shift our attention to the December measurement sessions conducted — during the last phase of the tremendous dust storm in 1971, when clouds obscured almost the entire surface of the planet for several months. In contrast to the high latitude clouds, these clouds were decidedly dust clouds rather than condensation clouds. In order to explain the thermal radiation profile of 15 December, considerably larger values for the integral albedo, i.e., 0.35 for the dark regions (Mare Cimmerium) and 0.40 for the light regions at latitudes south of  $L = -20^\circ$ , are required. In the equatorial zone an albedo of 0.50 is required. The albedo of Mars during the dust storm was actually larger than the albedo of the light regions under normal conditions [32, 36], but the difference is evidently not as large as would be required to explain the results obtained. In the  $1.4 \mu$  range the reflectivity of the continent was altogether 15% greater than on 16 and 28 February [32], and, when the wavelength is reduced, this increase in intensity observed during the dust storm dropped [36]. Thus the integral albedo also could not have increased by more than 15% in relation to its normal value of  $A = 0.25$ .

/24

We introduced a correction for atmospheric absorption for the December passes by using the standard procedure (see Section 4), which takes into account only the 15 micron  $\text{CO}_2$  range. It is obvious that aerosols during the dust storm could have accounted for the additional decrease, and, at first glance, it

seems entirely possible to bring the brightness temperatures of the surface more in line by increasing the correction for the atmosphere. However, this formally possible alternative can hardly be put into practice in our case. And in actuality a large, real absorption of solar radiation occurred in the Martian dust clouds. In addition, their optical density in true absorption is considerably larger for the solar radiation than for the planetary [14, 35, 37]. Under these circumstances the Martian dust clouds should lead to an actual drop in temperature and to the appearance of a unique "anti-greenhouse" effect [14, 35, 37, 38]. During the earlier stages of the dust storm, this effect was considerably more pronounced, as observations from Earth (in October 1971 [39]) and the Mariner observations (in November [11]) have shown. The drop in surface temperature was accompanied by an increase in atmospheric temperature [40]. The picture of the Martian atmosphere's thermal conditions during the dust storm in a certain sense is the opposite of the greenhouse effect in the atmosphere of Venus, and from this there has arisen the temptation to introduce in this case the term "anti-greenhouse effect". A semi-quantitative analysis of this analysis of this phenomenon is given in the paper by A. F. Ginzburg [38].

If we dispense with the correction for the atmosphere, then the observed flux is the total outgoing flux from the planet (surface radiation, weakened by the atmosphere plus the radiation of the atmosphere). This flux is smaller than is required under the conditions of instantaneous balance with the solar flux. This must be the case if some portion of solar radiation is trapped by the atmosphere, since its thermal inertia is large [24]. A part of the energy trapped during the day is emitted again at night, and the brightness temperature at night should have risen during the dust storm. Unfortunately, our sessions contained too few night measurements in order to confirm or deny this prediction. The night portion of the 15 December session does not show any temperature —increase, but this could be the result of the superposition of horizontal heterogeneities in the properties of the dust clouds (for instance, of an increase in the integral albedo during movement to lower latitudes).

/25

In absolute value the optical width of the dust clouds during the December sessions could not have been large in the 8 to 40  $\mu$  wavelength range which is of interest to us. According to [35] the width would have been on the order

of 0.1. This value was obtained by extrapolating from the visible and near-infrared ranges toward the greater wavelength. The very fact that the form of the radiometric profile obtained in general is the same as for a planet devoid of atmosphere, means that the optical thickness of the latter is small for thermal radiation. At [Translator's Note: This appears to be  $T > 1$ ] the midday maximum would have been strongly shifted, and a sharp increase in the amplitude of the daily temperature variations would have occurred.

The atmosphere's transparency for the 8 to 40  $\mu$  range thus turned out to be sufficiently great even during the dust storm, or at least during the period of its peak stage in December. The values of the thermal inertia parameter of 0.006 - 0.008 at higher integral albedo values turned out to be favorable to a formal interpretation of the thermal flows observed in December. It is difficult to explain the temperature increase in the Cerberus region near the terminator as the result of any atmospheric effect. Here an increase in the thermal inertia of the soil is most likely to take place. The theoretical temperatures in the area of the terminator are too insensitive to albedo changes (see Figures 7 and 10) to be able to attribute the observed effect to them. /26

If one shifts one's attention from 15 December to 27 December and 9 January, the integral albedo values which are necessary for the model representation of the observation decrease approach normal values (0.15 and 0.25), which are typical for the February sessions. The radiometric and photometric profiles of 9 January differ very little from the February profile. We note, however, that in Syrtis Major during the 27th December session the values which are obtained for thermal inertia (0.006) are twice as large for 16 February (0.004). It is possible that we are dealing here with the effect of local horizontal heterogeneities in the soil (see Section 8) which can lead to an increase in the effective value of the thermal inertia during the night in comparison with the day. Mare Erythraeum and Margaritifer Sinus in both sessions (27 December and 16 February) were observed by day, and in this case the inertia values obtained were close.

During the 15 December and 9 January sessions, negative correlation between the thermal and reflected radiation was observed, and individual deviations

from this general rule also occurred. As an example of this type of deviation, it is possible to point out trough I on the thermal profile of 9 January which agrees with the reflected profile trough. Here the paths cross a large crater (Figure 4 from [32]).

#### 8. The Thermal Properties and Mechanical Structure of the Martian Soil

The basic characteristics of all of the radiometric profiles examined in the previous section are represented satisfactorily by the theoretical models of a homogeneous semi-limitless layer at the parameter value

$$I = 0.006 \pm 0.002 \text{ cal cm}^{-2} \text{ sec}^{-1/2} \text{ deg}^{-1} \quad (14)$$

and this agrees well with the results of other authors [4, 7, 8, 9] except for /27 Leovy [6], who found  $I = 0.0015\text{--}0.0024$ . Leovy used the linearized form of equation (10), and this is evidently too much of a simplification.

Figure 15 shows the densities of various types of rock according to the data of work [41] in the function  $I_0$  thermal inertia in a vacuum. The values obtained for thermal inertia (the straight vertical line A) correspond will to pumice. The dependency of  $I_0$  on pressure is negligibly small for pumice. But a second variation is possible. If the soil is in a sintered state, one must recalculate thermal inertia from its Martian pressure of 6 mb to a vacuum, — during which process the thermal inertia will be reduced by approximately 3 times, and we obtain thus the value range B which corresponds to sintered basalt and granite. Thus we shift to two variations for the Martian soil:

- A - a porous nature such as pumice (density  $0.85 \pm 0.25 \text{ T to the centimeter}^{-3}$ ),
- B - sintered state (density  $0.2 \pm 2 \text{ grams per centimeter}^{-3}$ ).

It follows that there is sintered material on the surface independently of other observations (dust storms, dune-type formations, the presence of changes related to winds, see [42]). Therefore version B seems much more probable than A.

The small distribution of the values  $I = 0.006 \pm 0.002 \text{ cal cm}^{-2} \text{ sec}^{-1/2} \text{ deg}^{-1}$  is evidence of the rather high degree of homegenity of the Martian soil, at least up to scales on the order of several tens of kilometers. There are no indications of fixed rock types which occupy any area comparable to the radio-meter's field of view. No signs of endogenic heat were observed at all.

There are no systematic differences in thermal inertia between seas and continents (despite the conclusions of Morrison et al [7]). The zone of increased thermal inertia which were pointed out in the previous sections are apparently associated with several large craters which were crossed by the measurement passes. The compact thermal region of Cerberus, which is characterized by an increased value of  $I$ , is also relative to a large number of craters. It is possible that the increase is associated with the larger average size of the particles on the inclined crater embankments than are found on level surfaces. /28

If one knows  $I$ , it is possible to estimate the thermal conductivity and the penetration depth of a thermal wave  $\ell = \sqrt{\frac{\kappa}{\rho C \pi}}$  if  $P$  and  $C$  are assigned. The thermal volume per unit of mass  $C$  for terrestrial rocks is normally within the limits of 0.25-0.22 cal grams<sup>-1</sup> deg<sup>-1</sup> [41]. These data refer to the temperature range of 300 to 500° K. In the 200 to 300° K range which is of interest to us, the thermal volume will be somewhat smaller. We can take as an average value

$$C = 0.19 \pm 0.02 \text{ cal g}^{-1} \text{ deg}^{-1} \quad (15)$$

For the density of solar type B, we have the value

$$\rho = 1.2 \pm 0.2 \text{ g cm}^{-3} \quad (16)$$

It would be very attractive to use the densities obtained according to the measurements of the planet's radial emission during the same passes using the Mars-3 radio telescope [43]. In addition to the intensity on the three centimeter wavelength, the radio telescope measured the polarization, whence according to the formulas of Frenel' [Translator's Note: As Transliterated], a dielectrical constant is obtained which, in turn, is rather strongly associated with density. However, these results are first not free of errors which are caused by the unevenness of the surface, and second, they are related to layers which are located considerably deeper than the thermal wave penetrates (there are no daily variations in brightness temperature on the three centimeter wavelength). Obviously the density values in the surface layer which have been obtained on the basis of infrared observations (as was done above for thermal inertia) are more reliable.

If we accept as an average value  $I = 0.006 \text{ cal} \cdot \text{centimeters}^{-2} \cdot \text{sec}^{-1/2}$  /29  
 $\text{deg}^{-1}$ , then the thermal conductivity

$$K = 1.06 \cdot 10^{-4} \text{ cal deg}^{-1} \text{ cm}^{-1} \text{ sec}^{-1} \quad (17)$$

and the penetration depth of the thermal waves

$$\ell = \sqrt{\frac{K}{\rho c}} = 4.4 \text{ cm.} \quad (18)$$

The thermal conductivity of sintered rock depends on the pressure and the particle size. Laboratory investigations which have been carried out on sintered silicate materials (see [6, 41]) give the thermal conductivity value we need for a particle diameter of

$$d \approx 0.25 \text{ mm}$$

for a pressure of 6 mb. The photometric properties of the surface of Mars in the visible and near-visible infrared ranges require the use of particles of considerably smaller dimensions (about  $1 \mu$ ). It is possible that a hierarchic type of structure occurs: the large particles of grains of sand which are composed of smaller particles [44]. Table 1 gives, in addition to the average values above, also extreme values caused by the scattering of  $I$ ,  $c$  and  $p$ . We see that scattering is possible in the thermal conductivity coefficient and in the average particle size coefficient by approximately 2 times from the average value and in the penetration depth of the thermal waves by approximately 1.5 times.

The penetration depth of an electrical wave in silicate materials depends on the actual composition of the material, but, in the range which is of interest to us, it does not exceed 0.1 millimeters. It is considerably smaller than the penetration depth of a thermal wave, and the generally accepted assumption that the surface radiates directly does not raise any doubts.

The hypothesis on silicate composition is affirmed by observations of the spectra of Mars which were obtained by the infrared spectrometer on Mariner-9 during the dust storm [16]. These spectra show bands of absorption which are specially characteristic of silicates. This does not, however, refute the presence of an admixture of limonite  $\text{Fe}_2\text{O}_3 \cdot \text{H}_2\text{O}$  which is necessary to explain the polarimetric observations and the spectro-photometry in the  $0.4\text{--}3.5 \mu$  range (see for instance [25]).

TABLE 1. THERMAL PARAMETERS AND PARTICLE DIAMETER  
OF THE MARTIAN SOIL

Parameter	Average Value	Minimum Value	Maximum Value
Thermal Inertia $I (Kpc)^{1/2}$ (cal deg <sup>-1</sup> cm <sup>-2</sup> sec <sup>-1/2</sup> )	0,006	0,004	0,008
Thermal Volume C (cal g <sup>-1</sup> deg <sup>-1</sup> )	0,19	0,17	0,21
Density P (g cm <sup>-3</sup> )	1,2	1,0	1,4
Thermal Conductivity K, (cal deg <sup>-1</sup> cm <sup>-2</sup> sec <sup>-1/2</sup> )	$1,6 \cdot 10^{-4}$	$6,4 \cdot 10^{-5}$	$3,8 \cdot 10^{-4}$
Penetration Depth of Thermal wave $\ell$ , cm	4,4	2,7	6,5
Average Particle dimension d, cm	0,025	0,01	0,05

Commas indicate decimal points.

The interpretation of our measurements is based on the model of a solar homogeneous layer which is horizontally and vertically semi-unrestricted. Possible effects of vertical heterogeneity have been discussed earlier [9]. It was shown that a doubling of the temperature conductivity  $K$  below 2 centimeters causes a change in the calculated temperatures of  $t_{PC}$  not more than 4°, while the night temperatures change considerably.

The horizontal heterogeneities are apparently much more considerable, and it is considerably more difficult to evaluate their role quantitatively. Heterogeneities on a large (in comparison to the field of view) and a small scale should have different effects. The former can cause either an apparent decrease in  $I$  or increase depending on which part of the radiometric profile (the morning or the evening) the neighboring regions are located, one of which for any reason is warmer than the other: we are not always able to separate temporal changes from geographical. From the methodological point of view, it would be more correct to obtain thermal charts of limited surface area for different times of the day, but we did not have a free choice in this question. For the given type of orbit, it was impossible to do this.

/31

Heterogeneities on small scales (much smaller than the field of view) occur because of the fact that at night the temperatures are higher than in the homogeneous models since at this time of the day the areas with an increased  $I$  make the greatest contribution to thermal radiation, and during the day the relative contribution of these areas is smaller, and as a result the amplitude for the day can turn out to be smaller. Horizontal heterogeneity of this type is the cause of the fact that the values for  $I$  obtained at night and in the evening will be greater than near mid-day. The values of  $I$  for Syrtis Major of 27 December (0.008) and 16 February (0.004) can serve as examples. It is doubtful that in the given case this difference can be explained by the atmosphere, although this possibility cannot be fully ruled out (see Section 6). This type of contradiction can be regarded rather as an indication of the existence of significant heterogeneities on a small scale (no greater than 10-20 kilometers), and therefore it would be very important to increase spatial resolution in future experiments.

#### 9. Comparison with the Results of Mariner-9

The preliminary report on the results of the infrared radiometric experiment on Mariner-9 [45] became available to us after this work had already been completed. /32

The temperatures measured in both experiments on dates near to each other and in the same areas, as a rule, agree well. The conclusions coincide in their basic details: the American authors also note the absence of a correlation between the albedo and thermal inertia, low surface temperatures during the dust storms, and the lack of any sign of endogenic heat. In addition, since they possess material which was considerably greater in volume, they observed individual areas the thermal inertia of which was increased: the maximum value of the constant  $I$  in these regions reaches  $0.017 \text{ cal cm}^{-2} \text{ sec}^{-1/2} \text{ deg}^{-1}$ , and this corresponds to an average particle size of approximately 5 mm. The lower limits of the constant  $I$  in both series of measurements is the same as  $0.004 \text{ cal deg}^{-1} \text{ cm}^{-2} \text{ sec}^{-1/2}$ .

The authors would like to thank M. Kh. Akhmedeyev, V. Vdovin, B. S. Kunashev, A. M. Kasatkin, L. S. Kremenchugskiy, E. M. Luchnikova, G. M. Petrov,

N. V. Temana, G. V. Tomasheva, V. D. Filipkov, K. A. Tsoy, O. V. Yablonska, and other people who have given us considerable help during the various stages of completing this work.

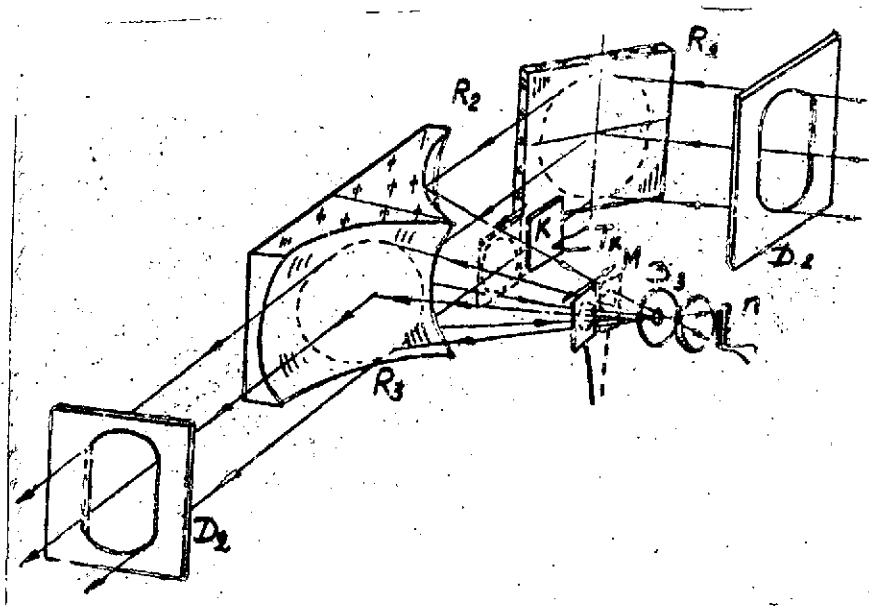


Figure 1. The Optical Diagram of a Radiometer.

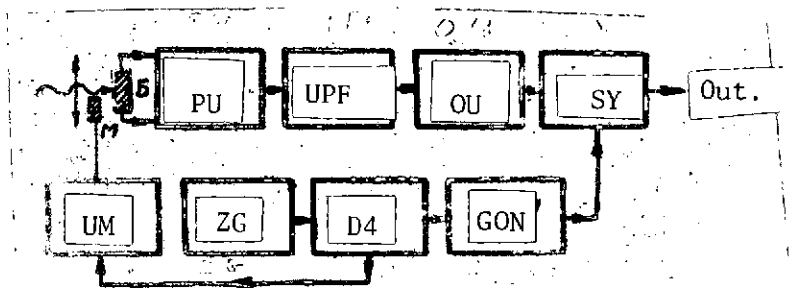


Figure 2. A Functional Electrical Diagram.

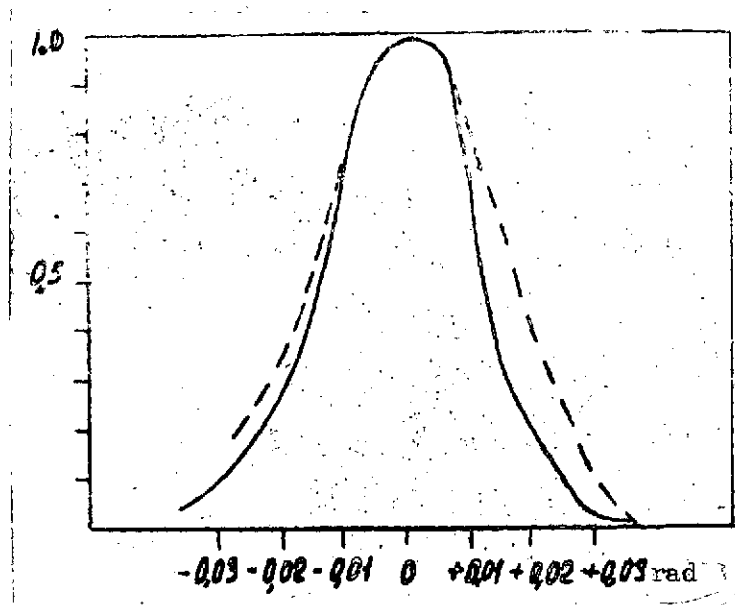


Figure 3. A Directivity Diagram in Two Mutually Perpendicular Directions.

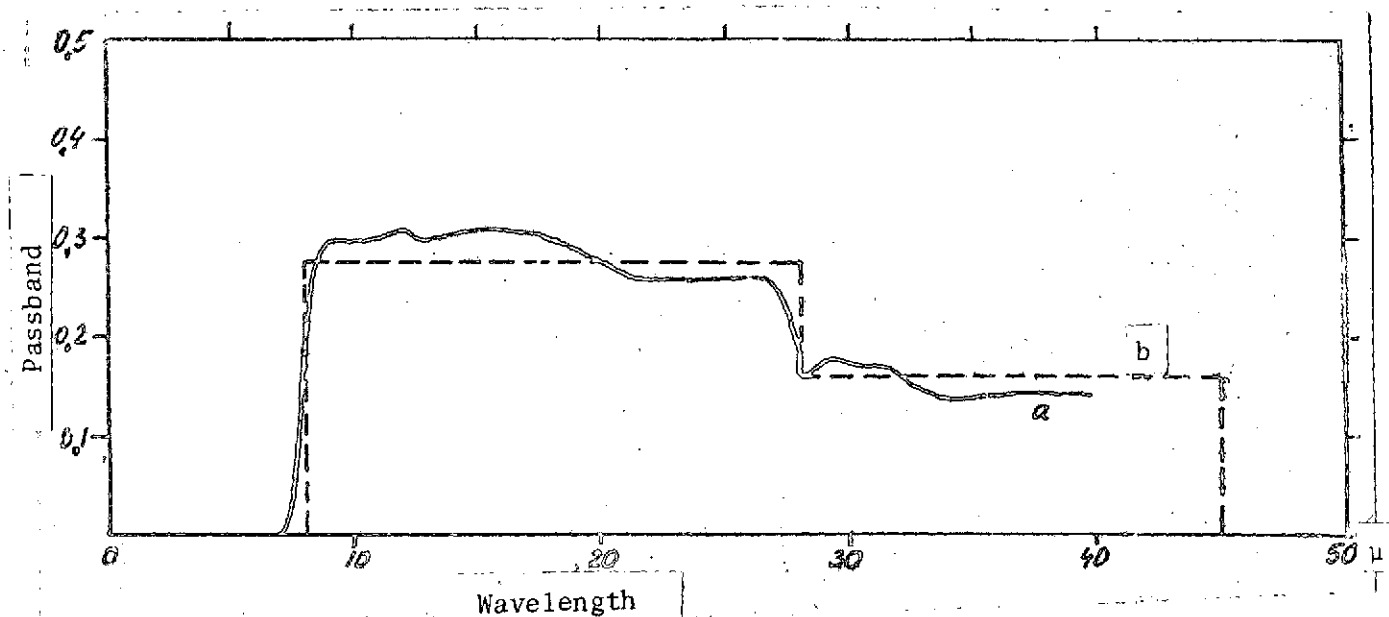


Figure 4. A Band Pass Curve of a Filter: a) Measured, b) Idealized (Accepted While Computing the Calculated Calibration Curve and the Correction For the Atmosphere).

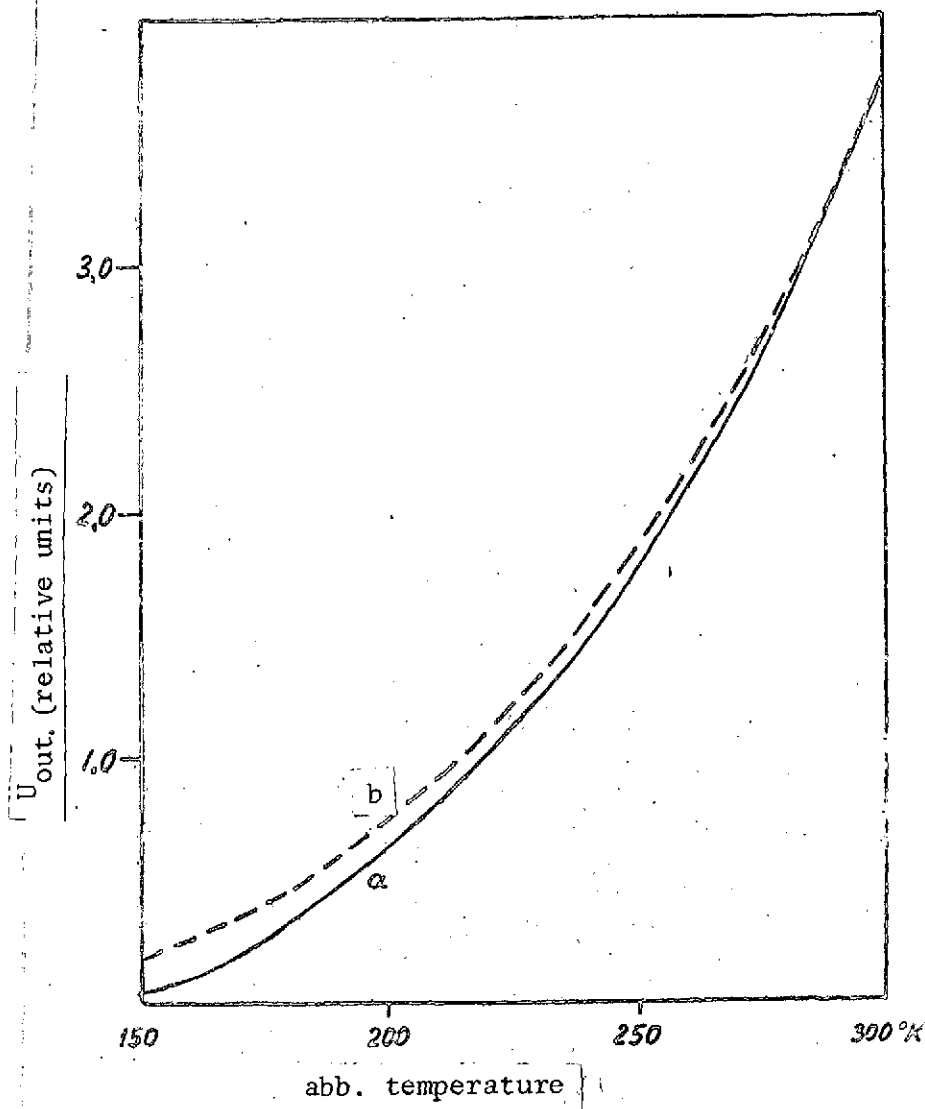


Figure 5. A Calibration Curve (the Output Signal as a Function of Intensity Temperatures)- Measured (a) and Calculated (b).



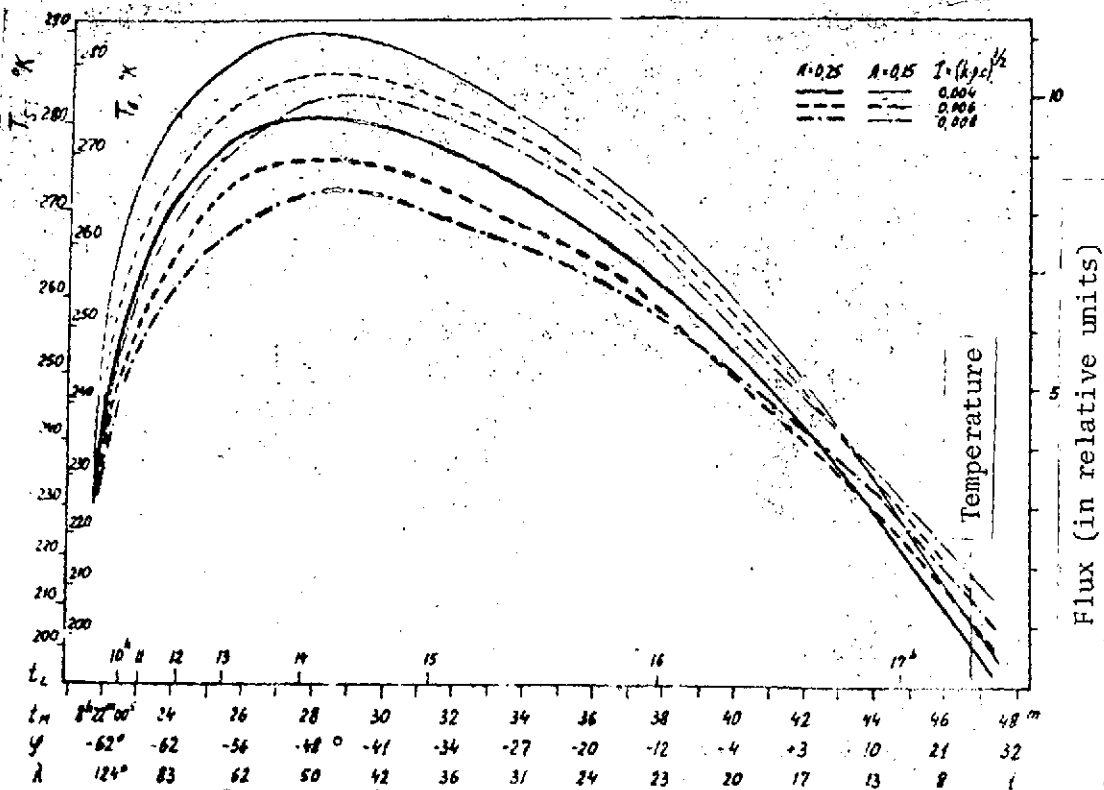


Figure 7. Theoretical Temperatures  $T_b$  and  $T_s$  Computed For the Paths of 9 January 1972 at Two Albedo Values ( $A = 0.15$  and  $0.25$ ) for Three Parameter Values (KPC) to the  $1/2$  Equals  $0.004$ ,  $0.006$ , and  $0.008 \text{ cal cm}^{-2} \text{ sec}^{-1/2} \text{ deg}^{-1}$ . The axis of the abscissa are Moscow time  $G_m$  and the local solar time  $T_1$  which correspond to it, as well as latitude  $L$  and longitude  $\lambda$  on Mars. Emissitivity is  $E = 0.9$ .

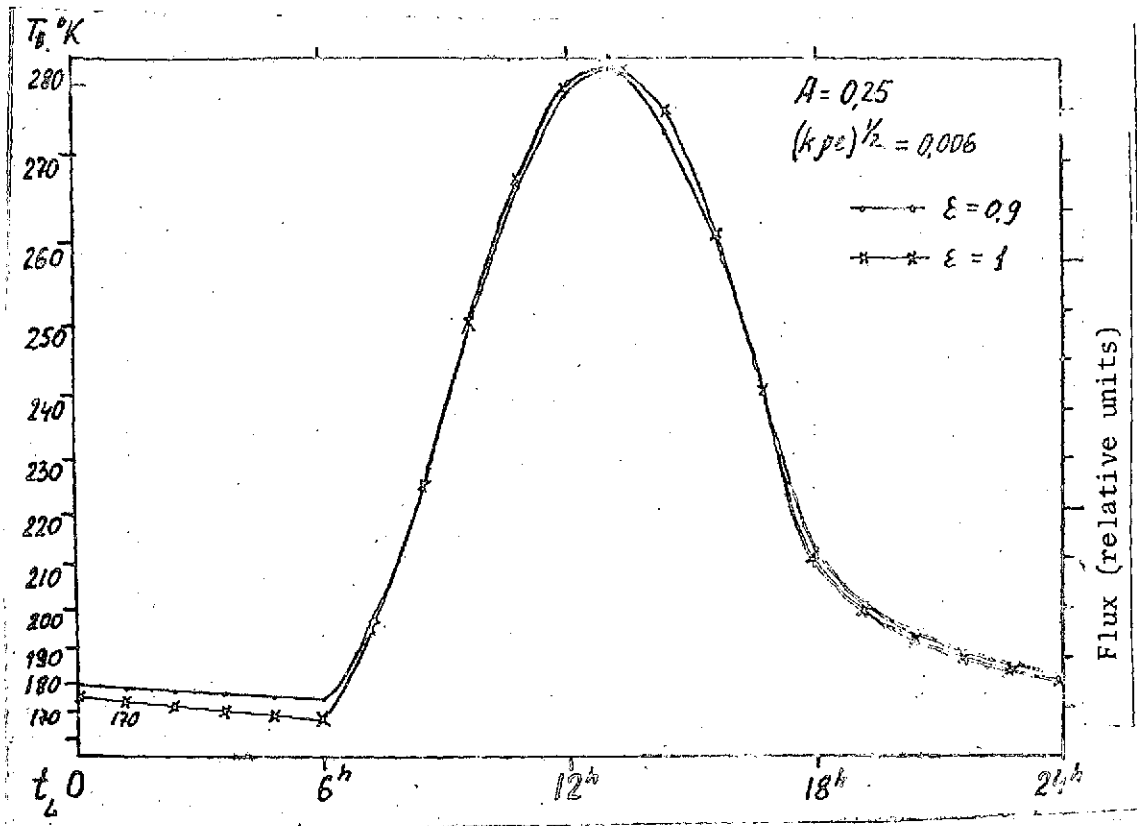


Figure 8. The Daily Course of Brightness Temperature  $T_b$  at the Equator Calculated For Regions With an Albedo of  $A = 0.25$  and a Thermal Inertia of (KPC) to the  $1/2$  Equals  $0.006 \text{ cal cm}^{-2} \text{ sec}^{-1/2} \text{ deg}^{-1}$  at 2 Emissitivity Values of  $E = 0.9$  and  $1.0$ .

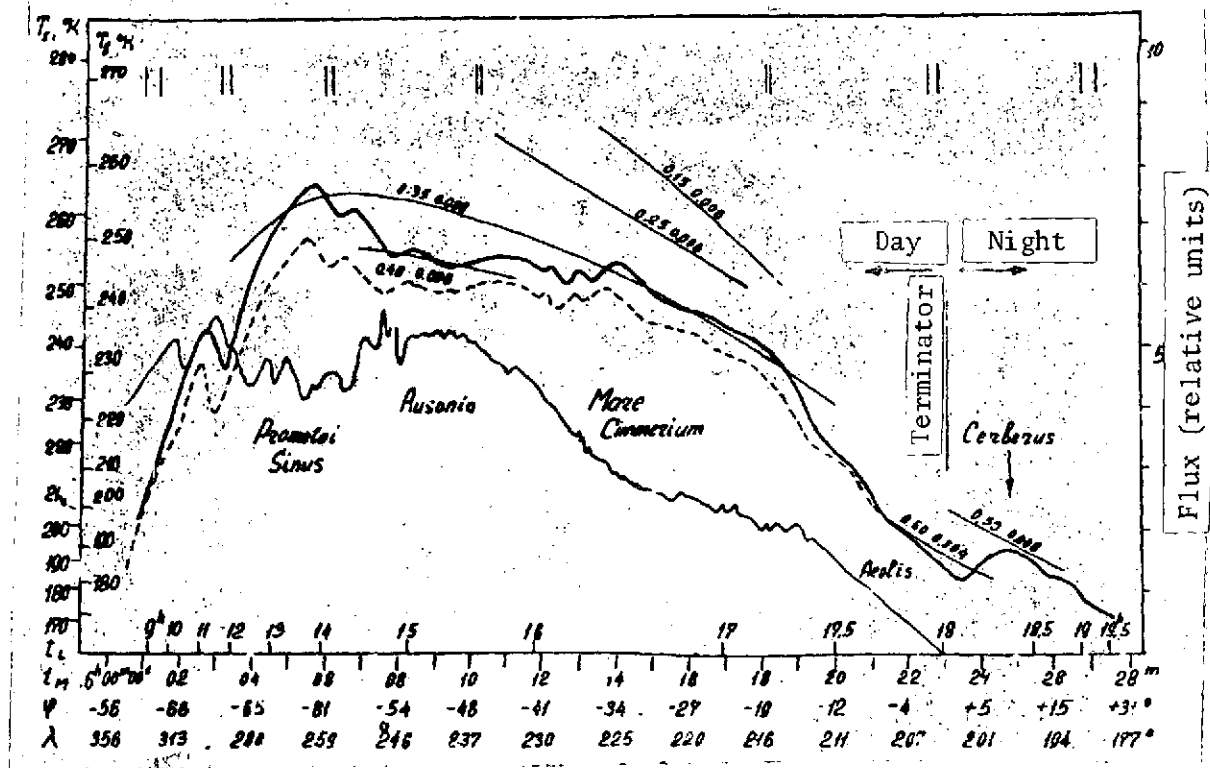


Figure 9. Brightness Temperature  $T_b$  and Kinetic Temperature  $T_s$  For the Surface of Mars on the 15 December Session. Moscow time is on the axis of the abscissas  $T_m$  local solar time on Mars is  $T_1$ , latitude is scrip S and longitude is  $\lambda$ . Along the axis of the ordinates to the left of  $T_b$  and  $T_s$ , on the right is the flow accepted in the 8th to 40  $\mu$  band in relative units. The vertical hatching indicates the width of the instrument profile of the radiometer (in angular measurement it is constant, on the  $T_m$  scale it is varied). The solid thick line is flow,  $T_b$  and  $T_s$  after introducing corrections for the atmosphere and the angular dependency of emissivity, the dotted line is the measured flow (without correction) the thin solid line is the brightness of Mars in the spectral range around  $\lambda = 1.4 \mu$  (reflected solar radiation). The sections of the curve with numeral designation are the temperatures which correspond to the calculated model of the surface (the albedo A and the thermal inertia  $I = (KPS)^{1/2}$  are indicated).

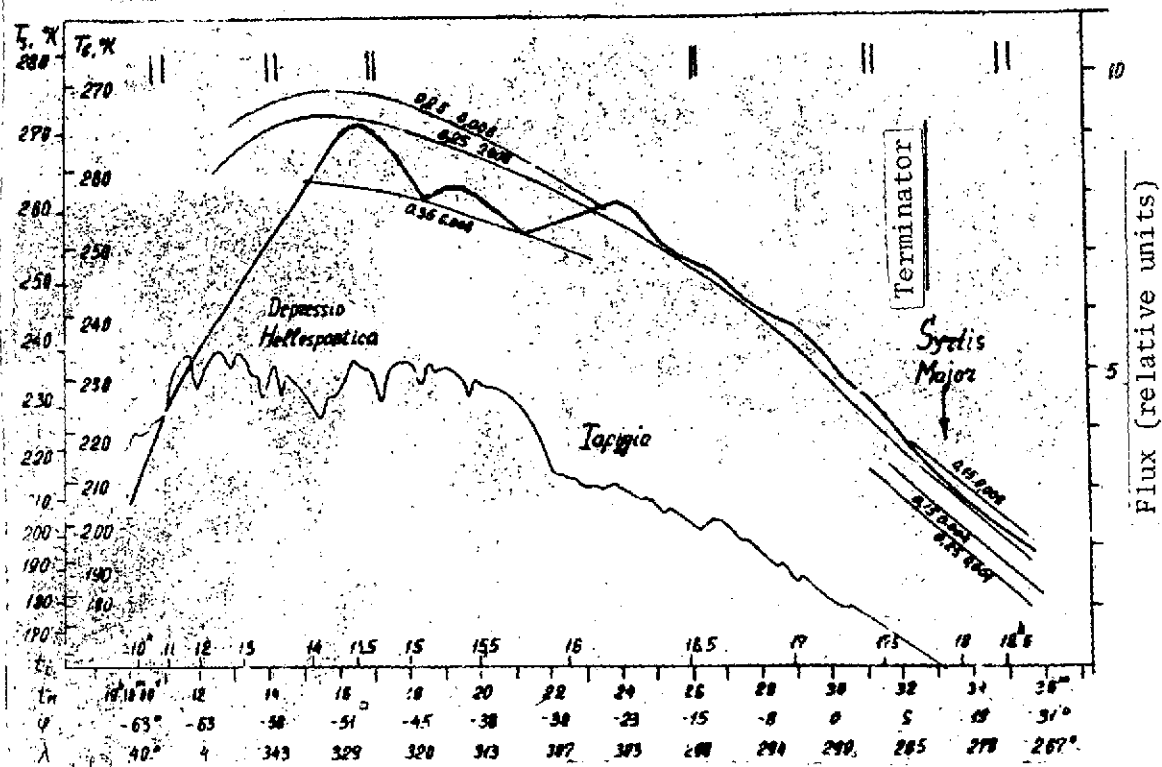


Figure 10.  $T_b$  and  $T_s$  on the 27 December Sessions.  
Measured the same as Figure 9.

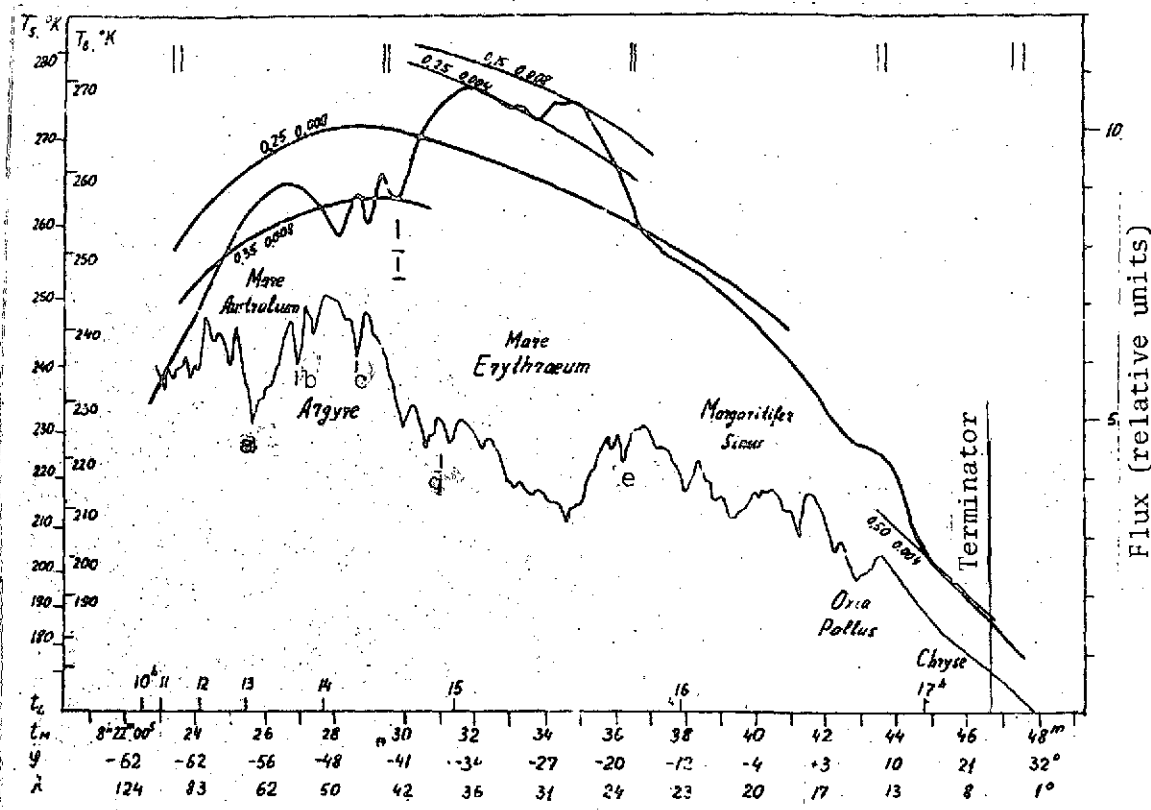


Figure 11.  $T_b$  and  $T_s$  on the 9 January Session. Measured the same as Figure 9. Individual details are indicated for the profiles of 8-40 and  $1.4 \mu$  which were mentioned in the text.

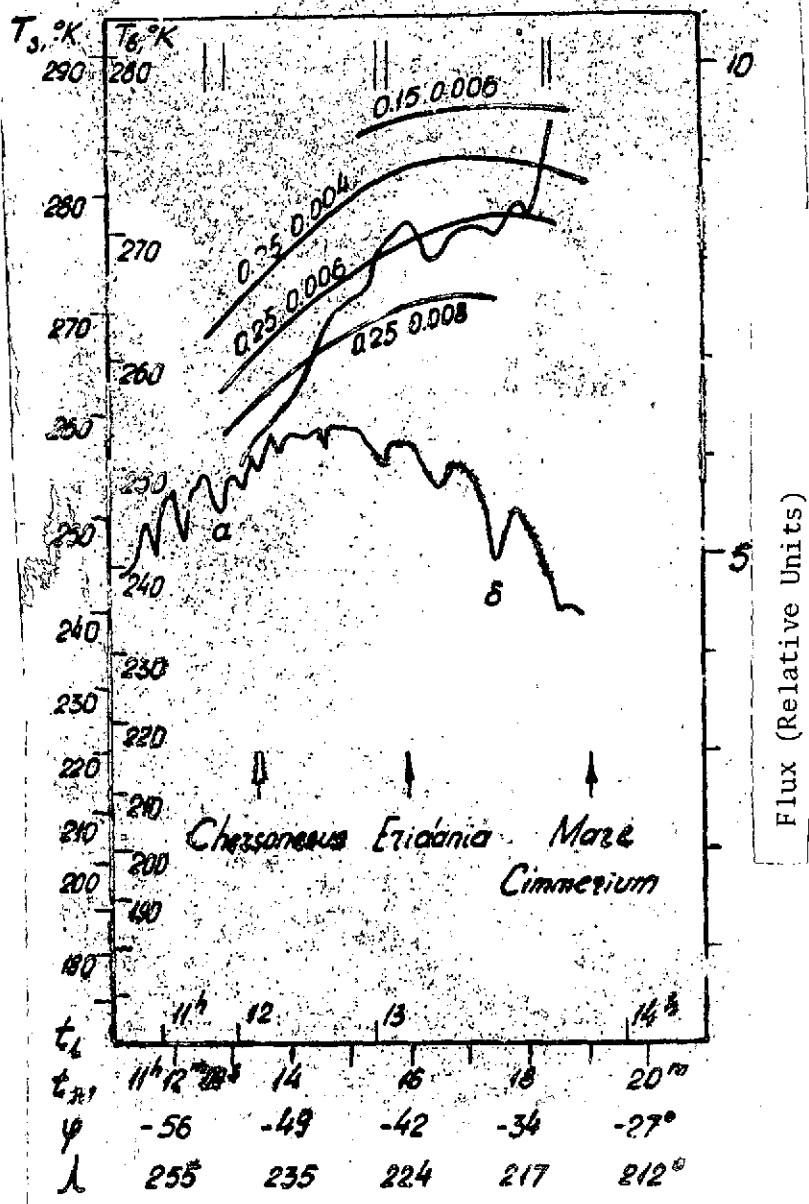


Figure 12.  $T_b$  and  $T_s$  on the 3 February Session. Measured the same as Figure 9.

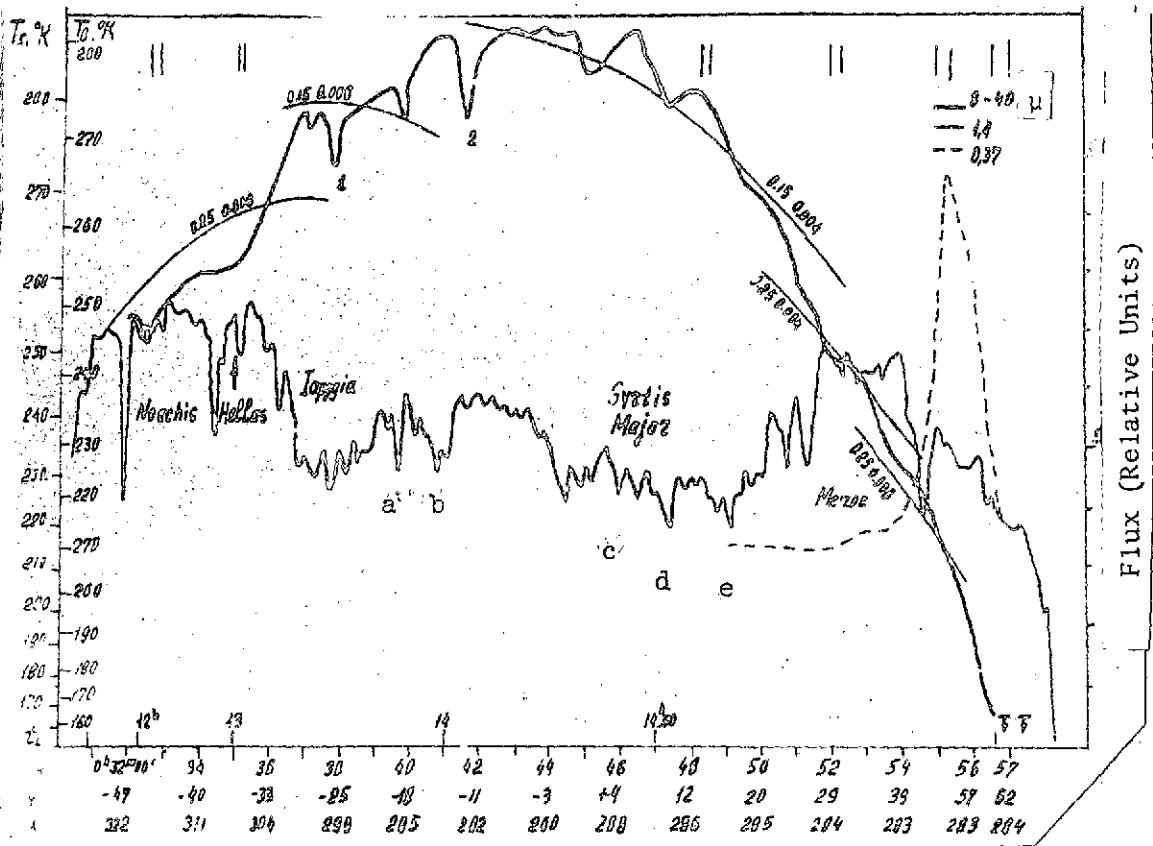


Figure 13.  $T_b$  and  $T_s$  on the 16 February Session.

The arrow indicates the photometric profile in a narrow spectral range around 3700  $\text{\AA}$ . The other symbols are the same as in Figure 9.

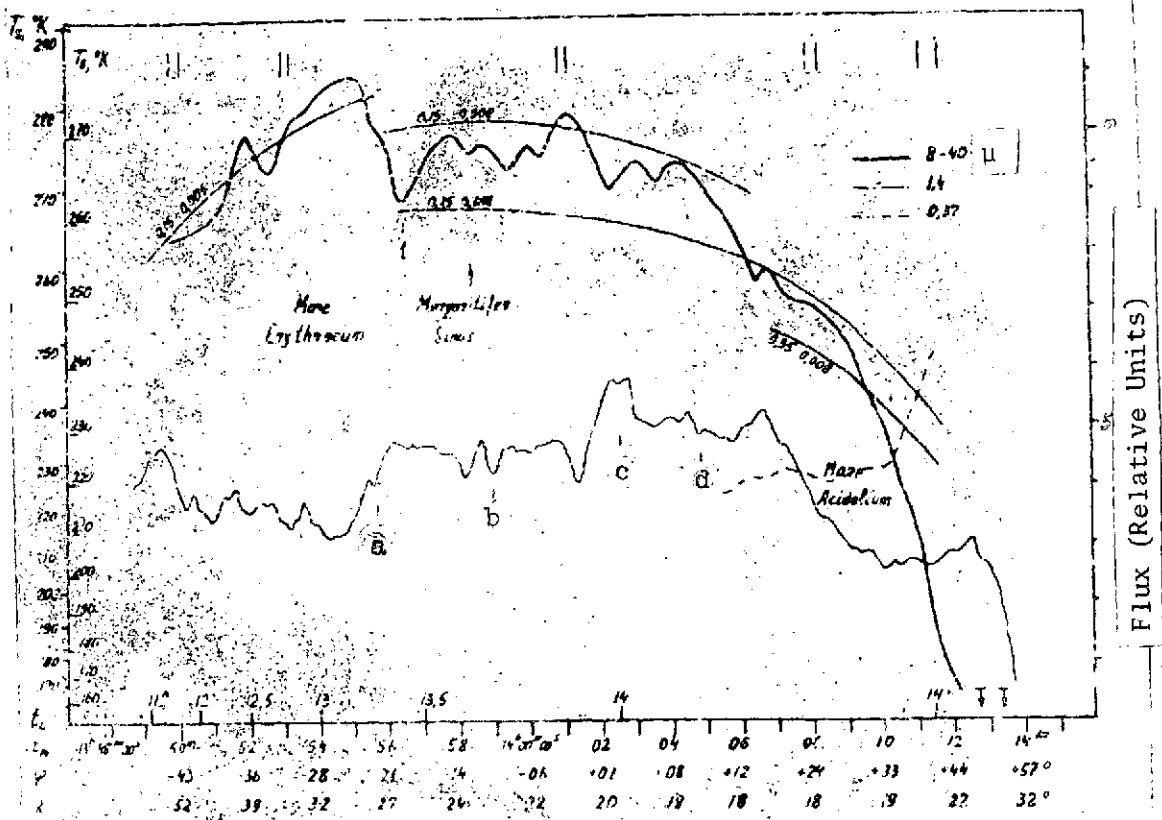


Figure 14.  $T_b$  and  $T_s$  on the 28 February Session.  
Legend the same as in Figure 9.

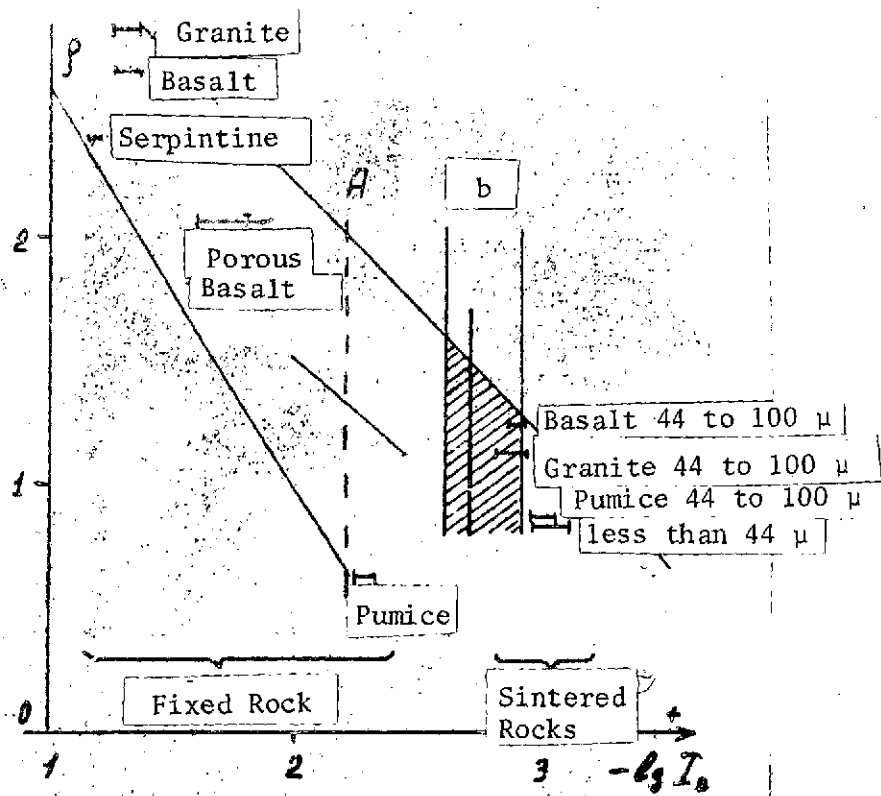


Figure 15. Density  $\rho$  and Thermal Inertia Parameter  $I_0$  (in a vacuum) For Rocks of Various Types (According to the Data of [41]). A is the observed thermal inertia, B is related to a vacuum.

1. Coblentz, W. and C. O. Lampland, *Lowell Obs. Bull.*, Vol. 3, p. 91, 1923; *Popular Astron.*, Vol. 32, p. 546, 1924.
2. Pettit, E., in the collection: *Planety i Sputniki* [Planets and Satellites], edited by Dzh. Koyper and V. M. Middlkerst, IL Press, 1963.
3. Sinton, W. and J. Strong, *Astrophys. J.*, Vol. 131, p. 459, 1960.
4. Sinton, V. M., in the collection: *Planety i Sputniki* [Planets and Satellites], edited by Dzh. Koyper and B. M. Middlkerst, IL Press, 1963.
5. Moroz, V. I., V. V. Davydov and V. S. Zheg[Translator's Note: Rest of name illegible], *Astron. Zh.*, Vol. 46, p. 136, 1969.
6. Leovy, C., *Icarus*, Vol. 5, p. 1, 1966.
7. Morrison, D., C. Sagan and J. B. Pollack, *Icarus*, Vol. 11, p. 36, 1969.
8. Leighton, R. R., B. C. Murrey, E. Miner and D. Schofield, *Science*, Vol. 153, p. 136, 1969.
9. Neugebauer, G., G. Muench, H. Kieffer and E. Miner, *A. J.*, Vol. 76, p. 719, 1971.
10. Moroz, V. I., L. V. Ksansomaliti, A. M. Kasatakin et al., *Doklady AN SSSR*, Vol. 208, p. 299, 1973.
11. Chase, S. C., H. Hatzenbeler, H. Kieffer and E. Miner, *Science*, Vol. 175, p. 308, 1971.
12. Gorodetskiy, A. K., E. F. Klimchuk and M. S. Malkevich, *Fizika Atmosfery i Okeana*, Vol. 5, No. 4, p. 355, 1969.
13. Ksanfomaliti, L. V., *Priboiy i Tekhnika Eksperimenta*, No. 4, p. 192, 1972.
14. Moroz, V. I. and L. V. Ksanfomaliti, *Icarus*, Vol. 17, p. 408, 1972.
15. Moroz, V. I. and L. V. Ksansomaliti, *Vestnik AN SSSR*, No. 9, p. 10, 1972.
16. Hanel, R. A., R. J. Conrath, W. A. Hovis et al., *Icarus*, Vol. 17, p. 423, 1972.
17. Hanel, R. A., B. J. Conrath, W. A. Hovis et al., *Icarus*, Vol. 12, p. 48, 1970.
18. Hovis, W. A., *Icarus*, Vol. 4, p. 425, 1965.
19. Hovis, W. A. and W. R. Callahan, *JOSA*, Vol. 56, p. 639, 1966.
20. Pettit, E. and S. B. Nicholzen, *Astrophys. J.*, Vol. 71, p. 102, 1930.
21. Wesselink, A. F., *BAN*, Vol. 10, p. 351, 1948.
22. Jaeger, J. C., *Austr. J. of Phys.*, Vol. 6, p. 10, 1953.
23. Jaeger, J. C., *Proc. Camb. Phil. Soc.*, Vol. 49, p. 355, 1953.
24. Gierash, P. and R. Goody, *Planet. Space Sci.*, Vol. 16, p. 615, 1968.
25. Moroz, V. I., *Fizika Planet* [The Physics of the Planet], "Nauka" Press, Moscow, 1967.
26. de Vaucouleurs, G. P., *Icarus*, Vol. 3, p. 187, 1969.
27. McCord, T. B., *Astrophys. J.*, Vol. 156, p. 79, 1969.
28. McCord, T. B., *Science*, Vol. 169, p. 1058, 1969.
29. Adams, J. B. and T. B. McCord, *J.G.R.*, Vol. 74, p. 4851, 1969.
30. McCord, T. B. and J. A. Westphal, *Astrophys. J.*, Vol. 168, p. 141, 1971.
31. McCord, T. B., J. H. Ellis and J. A. Westphal, *Icarus*, Vol. 14, p. 245, 1971.
32. Moroz, V. I., A. E. Nadzhip and V. S. Zhegulev, *Mars-3: Fotometricheskiye Profili Planety v Blishney Infrakrasnoy Oblasti Spektra* [Mars-3: Photometric Profiles of the Planet in the Near-Visible Infrared Range of the Spectrum], a preprint of the IKI AN SSSR, 1974.

33. "Mariner-9 Television-Experiment Team," *Sky and Tel.*, Vol. 44, p. 77, 1972.
34. Ksanfomaliti, L. V. and V. I. Moroz, *Mars-3: Fotoelektricheskaya Fotometriya s Uzkopolosnymi Fil'trami v Diapazone 3700-7000 A* [Mars-3: Photoelectric Photometry with Center-Band Filters in the 3700 to 7000 A Range], a preprint of the IKI AN SSSR, 1974.
35. Moroz, V. I., *Oblaka na Marse — Nekotorye Vывody iz Nablyudeniya na AMS "Mars-3"* [Clouds on Mars, Several Conclusions from the Observations of the Mars-3 Automatic Space Probe], a preprint IKI AN SSSR, 1974.
36. Barabashev, N. P., N. P. Kiselev and D. S. Lupishko, *Astron. Tsirk.*, No. 687, p. 3, 7 April 1972.
37. Moroz, V. I., L. V. Ksanfomaliti, A. M. Kasatkin and A. E. Nadzhip, *Kosmicheskiye Issledovaniya*, Vol. 10, p. 925, 1972.
38. Ginzburg, A. S., *Dokl. AN SSSR*, Vol. 208, p. 295, 1973.
39. Liberman, A. A., V. I. Moroz and G. S. Khromov, *Astron. Tsirk.*, No. 705, 5 June 1972.
40. Kliore, A., D. Cain and F. Fjeldbo, *Icarus*, Vol. 17, p. 484, 1972.
41. Wechsler, A. E. and P. E. Glaser, *Icarus*, Vol. 4, p. 335, 1965.
42. Sagan, C., J. Veverke, P. Fox et al., *Icarus*, Vol. 17, p. 346, 1972.
43. Basharinov, A. E., I. B. Drozdovskaya, S. T. Egorov et al., *Icarus*, Vol. 17, p. 450, 1972.
44. Moroz, V. I., *O Strukture Marsianskogo Grunta po Opticheskim i Infekrasnym Nablyudeniya* [On the Structure of the Martian Soil According to Optical and Infrared Observations], a preprint of the IKI AN SSSR, 1974.
45. Kieffer, H. H., S. C. Chase, Jr., E. Miner, G. Muench and G. Neugebauer, *J.G.R.*, Vol. 78, p. 4291, 1973.

/35

Translated for the National Aeronautics and Space Administration under Contract No. NASw-2485 by Techtran Corporation, P.O. Box 729, Glen Burnie, Maryland, 21061; translator, Thomas W. Appich, Jr.